



**CHALMERS**  
UNIVERSITY OF TECHNOLOGY

## **The Influence of Oxide-Scale Microstructure on KCl(s)-Induced Corrosion of Low-Alloyed Steel at 400 °C**

Downloaded from: <https://research.chalmers.se>, 2023-05-05 05:29 UTC

Citation for the original published paper (version of record):

Olivas Ogaz, M., Eklund, J., Persdotter, A. et al (2019). The Influence of Oxide-Scale Microstructure on KCl(s)-Induced Corrosion of Low-Alloyed Steel at 400 °C. *Oxidation of Metals*, 91(3-4): 291-310. <http://dx.doi.org/10.1007/s11085-018-9881-2>

N.B. When citing this work, cite the original published paper.



# The Influence of Oxide-Scale Microstructure on KCl(s)-Induced Corrosion of Low-Alloyed Steel at 400 °C

Mercedes Andrea Olivas-Ogaz<sup>1</sup> · Johan Eklund<sup>1</sup> · Amanda Persdotter<sup>1</sup> · Mohammad Sattari<sup>2</sup> · Jesper Liske<sup>1</sup> · Jan-Erik Svensson<sup>1</sup> · Torbjörn Jonsson<sup>1</sup>

Received: 26 July 2018 / Published online: 27 November 2018

© The Author(s) 2018

## Abstract

The high-temperature corrosion of low-alloyed steels and stainless steels in the presence of KCl(s) has been studied extensively in the last decades by several authors. The effect of KCl(s) on the initial corrosion attack has retained extra focus. However, the mechanisms behind the long-term behavior, e.g., when an oxide scale has already formed, in the presence of KCl(s) are still unclear. The aim of this study was to investigate the effect of the microstructure of a pre-formed oxide scale on low-alloyed steel (Fe–2.25Cr–1Mo) when exposed to small amounts of KCl(s). The pre-oxidation exposures were performed at different temperatures and durations in order to create oxide scales with different microstructures but with similar thicknesses. After detailed characterization, the pre-oxidized samples were exposed to 5%O<sub>2</sub> + 20%H<sub>2</sub>O + 75%N<sub>2</sub> (+KCl(s)) at 400 °C for 24, 48, and 168 h and analyzed with scanning electron microscopy, energy-dispersive X-ray spectroscopy, X-ray diffraction, and focused ion beam. The microstructural investigation indicated that Cl-induced corrosion is a combination of oxide thickness and microstructure, and the breakaway mechanism in the presence of KCl(s) is diffusion-controlled as porosity changes prior to breakaway oxidation were observed.

**Keywords** Pre-oxidation · Low-alloyed steels · Cl-induced corrosion · High-temperature corrosion

---

✉ Mercedes Andrea Olivas-Ogaz  
andrea.olivas@chalmers.se

<sup>1</sup> Department of Chemistry and Chemical Engineering, Environmental Inorganic Chemistry, High Temperature Corrosion Center, Chalmers University of Technology, 41296 Gothenburg, Sweden

<sup>2</sup> Department of Physics, Materials Microstructure, Chalmers University of Technology, 41296 Gothenburg, Sweden

## Introduction

Renewable fuels, such as biomass and waste, are attractive replacements for fossil fuels in heat and power production in order to achieve a sustainable society. However, in biomass- and waste-fired boilers, the fireside environment is known to be more corrosive than in fossil-fired boilers due to the high levels of reactive alkali- and chlorine-containing compounds in flue gas and deposits [1]. The superheater and waterwall areas are some, among others, of the affected parts where a corrosion attack may lead to failure and costly outages. For this reason, biomass and waste-fired boilers are often operated at a lower steam temperature, resulting in decreased electrical efficiency. In order for renewable fuels to replace fossil fuels, it is necessary to both lower the material costs and increase the efficiency of the production of power, which can be done by increasing steam temperatures and/or using less expensive materials, such as low-alloyed steels. Therefore, it is of great interest to gain better understanding of the corrosion mechanisms of low-alloyed steels in biomass- and waste-fired boilers.

The environment generated by the combustion of biomass and waste is very complex, and there are several factors involved in the corrosion attack on superheater materials. These factors include steel composition, the nature of the formed oxide scale/corrosion products, and the composition of deposits and flue gas. The corrosive environment in biomass- and waste-fired boilers is characterized by high levels of alkali and chlorine. Several studies have investigated the high-temperature corrosion of low-alloyed and stainless steels in the presence of alkali chlorides and other chlorine-containing compounds [2–15]. Reese et al. and Folkesson et al. [13, 15] have shown that alkali chlorides (NaCl, KCl) may have an important influence on the oxidation of low-alloyed steel (Fe–2.25Cr–1Mo), accelerating the oxidation rate at 500 and 400 °C. Jonsson et al. [14] have found that a KCl-induced corrosion attack initiates quickly and starts as early as at 355 °C. This has been suggested to be caused by the formation of eutectics that spread the deposited salt over the sample surface, in line with the phase diagram of FeCl<sub>2</sub>–KCl [14]. However, these studies have focused on the initiation of a corrosion attack on a clean metal surface, which would not be the normal case in a boiler. Reese et al. [15] have studied the effect of pre-oxidation on the NaCl acceleration of the rate of corrosion. Those authors have suggested that the thinner the oxide layer, the faster the reaction and diffusion of FeCl<sub>2</sub>. However, the oxide thicknesses investigated in that study were in the millimeter range, and the influence of microstructure was not investigated.

The oxidation of pure iron, FeCr model alloys and low-alloyed steels, is well documented in both dry and wet atmospheres containing oxygen [16, 17]. The outward-growing oxide consists of hematite and magnetite, while the Cr remains in the inward-growing scale [17]. This microstructure is assumed to be susceptible to a chlorine-induced attack. The mechanisms behind this phenomenon are still not fully understood, especially how chlorine is transported through the oxide scale. Several mechanisms have been proposed, including diffusion through cracks, pores, and along the oxide grain boundaries. The so-called active

oxidation mechanism suggests that chlorine penetrates through the oxide scale in the form of a molecule,  $\text{Cl}_2(\text{g})$  [3]. The chlorine forms metal chlorides when it reaches the oxide–metal interface. Due to their high vapor pressures, chlorides diffuse out toward the oxide–gas interface. Since the oxygen partial pressure increases closer to the gas/oxide interface, the metal chlorides transform into metal oxide and release  $\text{Cl}_2(\text{g})$ , which either penetrates back toward the metal or evaporates. The resulting metal oxide is porous, and therefore, it is less protective against corrosion attacks [3]. Folkesson et al. [18] have suggested that, in dry oxygen and in the presence of  $\text{HCl}(\text{g})$ , the formation of  $\text{Cl}_2(\text{s})$  is possible and, subsequently, so is its reduction to  $\text{Cl}^-$  ions. The same authors have also proposed that  $\text{Cl}^-$  ions form from the reaction of  $\text{KCl}(\text{s})$  with oxygen and water vapor, which releases  $\text{KOH}(\text{g})$  [13]. The transport of  $\text{Cl}^-$  ions through the oxide scale is proposed by Folkesson et al. [18] to take place along the grain boundaries of the oxide. However, very little is known about the influence of the oxide microstructure on chlorine-induced corrosion.

The aim of this study is to investigate the influence of oxide microstructure on chlorine-induced corrosion. This is achieved with a two-step exposure approach. First, well-controlled laboratory exposures were performed without  $\text{KCl}(\text{s})$  in order to pre-oxidize Fe–2.25Cr–1Mo steel. The pre-oxidation parameters were selected in order to obtain different oxide microstructures with similar oxide-scale thicknesses. In a second step, the well-characterized pre-oxidized samples were exposed in the presence and absence of small amounts of  $\text{KCl}(\text{s})$  at 400 °C in an environment containing 5% $\text{O}_2$  + 20% $\text{H}_2\text{O}$  + 75% $\text{N}_2$ . The morphology and microstructure of the corrosion products were characterized with advanced electron and ion microscopy, and the microstructure was linked to the  $\text{KCl}(\text{s})$ -induced corrosion response.

## Experimental Procedures

### Sample Preparation

The material used for this study was the Fe–2.25Cr–1Mo low-alloyed steel whose chemical composition is 0.1 C, 0.5 Mn, 0.3 Si, 0.9 Mo, 2.2 Cr, Fe-bal. An as-received 2 mm plate was cut into coupons with the dimensions of 15 mm × 15 mm. A hole of about 1.5 mm in diameter was drilled to facilitate sample handling. The samples were ground down to 320 grit on SiC paper and polished with 9, 3, and 1  $\mu\text{m}$  diamond suspension to achieve a mirror-like surface. After polishing, the samples were cleaned and degreased with acetone and ethanol in an ultrasonic agitation bath.

### Pre-oxidation

Before exposure to  $\text{KCl}(\text{s})$ , the samples were pre-oxidized in order to produce tailor-made oxide scales on the samples. The aim was to produce oxide scales with a similar total thickness but with different microstructures, i.e., the oxide grain size and

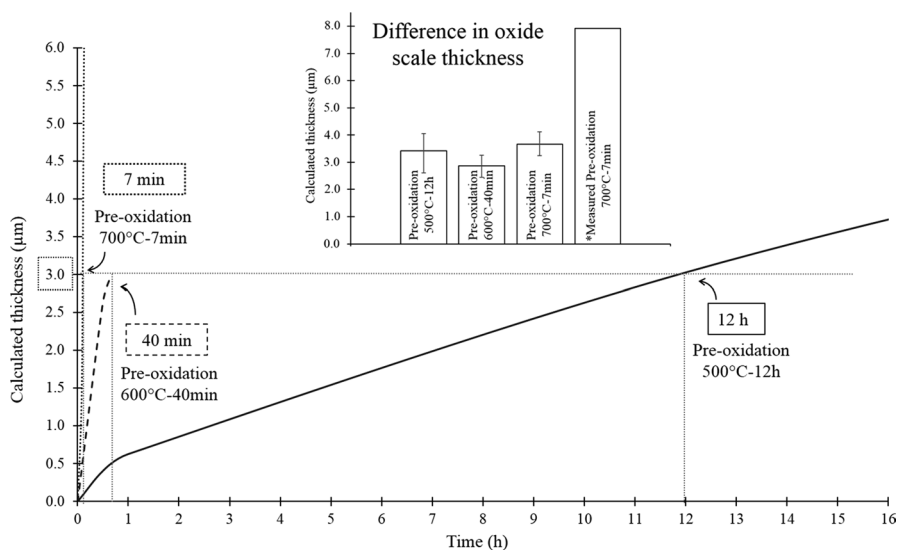


**Fig. 1** Pre-oxidation of Fe–2.26Cr–1Mo to 5%O<sub>2</sub> + 20%H<sub>2</sub>O + 75%N<sub>2</sub>: pre-oxidation time versus calculated thickness

**Table 1** Pre-oxidation parameters

Name	Temperature (°C)	Time	Atmosphere	kp (g <sup>2</sup> /cm <sup>4</sup> s)
500 °C-12 h	500	12 h	5%O <sub>2</sub> + 20%H <sub>2</sub> O + 75%N <sub>2</sub>	6 × 10 <sup>-12</sup>
600 °C-40 min	600	40 min	5%O <sub>2</sub> + 20%H <sub>2</sub> O + 75%N <sub>2</sub>	8 × 10 <sup>-11</sup>
700 °C-7 min	700	7 min	5%O <sub>2</sub> + 20%H <sub>2</sub> O + 75%N <sub>2</sub>	5 × 10 <sup>-06</sup>

thickness of each oxide layer. In order to achieve this, prior studies on iron and low-alloyed steels [13] [16, 17] and trial-and-error exposures were used to select the pre-oxidation parameters. The pre-oxidations were performed in tube furnaces at 500, 600, and 700 °C with running gas that consisted of 5%O<sub>2</sub> + 20%H<sub>2</sub>O + 75%N<sub>2</sub>. The pre-oxidation times were different for each temperature since similar thicknesses were intended. The thicknesses were calculated based on the mass gain after oxidation and were measured in ion-milled cross sections. A detailed explanation of the calculation of the oxide thickness is given by Lalgudi Srinivas [19]. A plot of calculated thickness as a function of oxidation time is shown in Fig. 1. Table 1 shows the chosen parameters and kp values of the pre-oxidation step.

### Exposure in the Presence of KCl(s)

After pre-oxidation, KCl(s) was deposited on the sample surfaces prior to exposure. This was done by spraying a saturated solution of KCl(s) in a 20:80 volume ratio water–ethanol mixture and dried with warm air. The amount of salt deposited on

each sample was about  $0.1 \text{ mg/cm}^2$ . Pre-oxidized samples without KCl(s) were also exposed and analyzed as a reference. The mass gains were recorded using a Sartorius<sup>TM</sup> balance with microgram resolution. All samples were kept in desiccators before and after exposure to prevent atmospheric corrosion.

The exposures were performed isothermally in horizontal silica tube furnaces at 400 °C. The exposure times were 24, 48, and 168 h. The reaction atmosphere consisted of  $5\% \text{O}_2 + 20\% \text{H}_2\text{O} + 75\% \text{N}_2$  with a flow rate of 2.5 cm/s parallel to sample surfaces. The gas flow was calibrated with a Bios Definer 220 M. In order to prevent any condensation of water in the system, all parts were kept over 100 °C. The samples were placed in the center of the furnace, mounted vertically on an alumina sample holder with a capacity for three samples.

## Experimental Techniques

Wide cross sections (in the millimeter range) of the corroded surfaces were prepared by dry cutting the samples with a low-speed diamond saw and subsequent broad ion-beam (BIB) milling with a Leica TIC 3X instrument operated at 6 kV. Prior to cutting, the samples were sputter-coated with gold, and a thin polished silicon wafer was glued on the surface in order to protect the oxide scale during cutting and to render a smooth cross-section after milling.

The samples were analyzed by means of scanning electron microscopy (SEM) and energy-dispersive X-ray spectroscopy (EDX) using an FEI Quanta 200 equipped with an Oxford Instruments X-Max<sup>N</sup> 80 T EDX detector and a Zeiss Ultra 55 SEM. The operation parameters were 10–20 kV using backscattered electrons (BSE) and secondary electrons (SE) detectors. Images of the oxide microstructures were obtained using focused ion beam (FIB) with ion-induced secondary electron imaging with an FEI Versa 3D DualBeam instrument operated at 30 keV and a beam current of 10 pA.

## Results

### Pre-oxidation

The aim of the pre-oxidations was to map out the oxidation behavior of the low-alloyed steel Fe–2.25Cr–1Mo in the temperature range of 400–700 °C to be able to design exposures in order to generate oxide scales with different microstructures with a similar thickness (a thickness of about  $3 \mu\text{m}$  was intended). Exposures performed at different temperatures were expected to generate different microstructures, i.e., the grain size and distribution of phases. The pre-oxidation parameters were selected based on the literature [16] and test exposures were performed at 500, 600, and 700 °C of the Fe–2.25Cr–1Mo alloy in the  $5\% \text{O}_2 + 20\% \text{H}_2\text{O} + 75\% \text{N}_2$  environment. The exposure times were predicted according to Fig. 1. The samples were exposed at 500 °C for 12 h, 600 °C for 40 min, and 700 °C for 7 min; see Table 1 for oxide-scale names and summarized details. The exposures resulted in

**Table 2** Calculated and measured thickness and grain size of pre-oxidation 500 °C-12 h, 600 °C-40 min, and 700 °C-7 min

	Calculated thickness (μm)			Measured thickness (μm)				Grain size (μm)		
	Average	Max.	Min.	Hematite	Magnetite	Spinel	Total	Hematite	Magnetite	Spinel
Pre-oxidation 500 °C-12 h	3.4	4.0	2.6	0.9	1.7	1.1	3.7	0.15	0.45	0.97
Pre-oxidation 600 °C-40 min	3.0	3.3	2.4	1.0	1.3	0.8	3.1	0.24	0.37	0.55
Pre-oxidation 700 °C-7 min	3.7	3.3	4.1	1.0	3.9	2.6	7.5	0.27	0.78	1.56

calculated thicknesses of the oxide scales of about 3–4  $\mu\text{m}$  (assuming scales consisting of magnetite) for all the pre-oxidized samples; see Table 2. The oxide-scale thicknesses were additionally investigated using SEM/BSE on millimeter-wide ion-milled cross sections, and the scale microstructure was characterized with ion-beam-induced secondary electron imaging in FIB systems; see Fig. 2. This technique provides distinct crystallographic orientation contrast in polycrystalline materials as a result of an ion-channeling effect and the different oxide phases were possible to identify through their difference in grain size [20].

### Pre-oxidation Performed at 500 °C

A large number of samples were exposed at 500 °C. The  $k_p$  value was calculated to be  $6 \times 10^{-12} \text{ g}^2/\text{cm}^4\text{s}$  and a 12-h exposure was selected to give the target thickness of the pre-formed oxide. The average mass gain after the 12-h exposure was  $0.49 \text{ mg}/\text{cm}^2$  ( $\pm 0.10 \text{ mg}/\text{cm}^2$ ), and the calculated average thickness was 3.4  $\mu\text{m}$  (2.6–4.0  $\mu\text{m}$ ). The surface morphology of the samples was homogeneous over the entire surface, and the sample was covered with large whiskers. The oxide-scale microstructure was investigated, and the interpretation of the microstructure has been based on earlier reported characterizations of oxide phases formed on low-alloyed steels and iron [16, 17, 21]. The oxide scales consisted of a top layer interpreted as hematite ( $\text{Fe}_2\text{O}_3$ ) and a middle layer of magnetite ( $\text{Fe}_3\text{O}_4$ ). The inner layer consisted of an iron chromium spinel ( $(\text{Fe,Cr})_3\text{O}_4$ ). All layers of the investigated areas had a uniform thickness even though the scatter in thickness between samples/areas was larger than the scatter in mass gain. The measured (SEM) total thickness of the oxide scale formed during pre-oxidation at 500 °C for 12 h was, on average, 3.7  $\mu\text{m}$ , with approximately 0.9  $\mu\text{m}$  of hematite, 1.7  $\mu\text{m}$  of magnetite, and 1.1  $\mu\text{m}$  of iron chromium spinel oxide ( $(\text{Fe,Cr})_3\text{O}_4$ ). This corresponds to about 25% hematite, 45% magnetite, and 30% iron chromium spinel. Pores were observed in the magnetite layer. The grain sizes measured for the hematite were about 190 nm. The grains

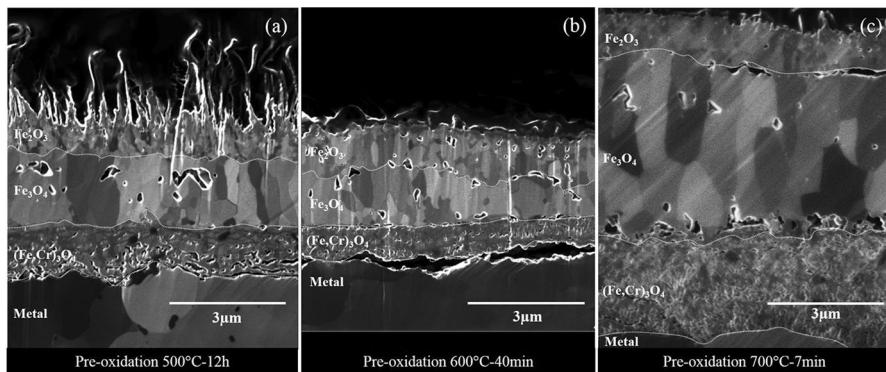


**Fig. 2** Cross sections of pre-oxidized Fe–2.25Cr–1Mo: pre-oxidations **a** 500 °C–12 h, **b** 600 °C–40 min, and **c** 700 °C–7 min (see parameters in Table 2); samples prepared with focused broad ion beam (BIB) milling and imaged with ion beam



of the middle layer of magnetite were measured in the horizontal and vertical directions since the grains formed were columnar-shaped. The magnetite grain sizes were 0.45  $\mu\text{m}$  (horizontal) and 0.84  $\mu\text{m}$  (vertical). The inward-growing spinel grain size was not possible to measure because the oxide grains could not be distinguished in all the pre-formed oxide scales.

### Pre-oxidation Performed at 600 °C

The  $k_p$  value was calculated to be  $8 \times 10^{-11} \text{ g}^2/\text{cm}^4\text{s}$ . An exposure time of 40 min was selected to give the target thickness of the pre-formed oxide. The average mass gain was 0.41  $\text{mg}/\text{cm}^2$  with a spread of  $\pm 0.06 \text{ mg}/\text{cm}^2$  with a calculated average thickness of 3.0  $\mu\text{m}$  (2.4–3.3  $\mu\text{m}$ ). The surface morphology showed a smooth surface and no indications of whisker formation. The oxide scales presented the same layers as the pre-oxidation at 500 °C. The measured thickness of the oxide scale was 3.1  $\mu\text{m}$  with approximately 1  $\mu\text{m}$  of hematite, 1.3  $\mu\text{m}$  of magnetite, and 0.8  $\mu\text{m}$  of iron chromium spinel ( $(\text{Fe,Cr})_3\text{O}_4$ ). This corresponds to 35% hematite, 40% magnetite, and 25% iron chromium spinel. Large pores were observed in the magnetite layer, and the measured grain sizes of the pre-formed hematite were about 240 nm. The magnetite grains were 0.35  $\mu\text{m}$  horizontally and 0.56  $\mu\text{m}$  vertically.

### Pre-oxidation Performed at 700 °C

Samples were additionally exposed at 700 °C. The  $k_p$  value at 700 °C was calculated to be  $5 \times 10^{-06} \text{ g}^2/\text{cm}^4\text{s}$  and a 7-min exposure was selected to give the target thickness for the oxide scale. After the 7-min exposure, the average mass gain was 0.52  $\text{mg}/\text{cm}^2$  with a spread of  $\pm 0.06 \text{ mg}/\text{cm}^2$ . The average thickness based on magnetite was 3.7  $\mu\text{m}$  (3.3–4.1  $\mu\text{m}$ ). The surface morphology was smooth/homogeneous, and no whiskers were visible. However, the thickness found for the oxide scale is not in agreement with the mass gain; see Fig. 2 and Table 2. The average thickness of the oxide scale was 7.5  $\mu\text{m}$ . The distribution between individual oxide layer thicknesses was 1  $\mu\text{m}$  for hematite, 3.9  $\mu\text{m}$  for magnetite, and 2.6  $\mu\text{m}$  for spinel oxide ( $(\text{Fe,Cr})_3\text{O}_4$ ). This corresponds to 15% hematite, 50% magnetite, and 35% iron chromium spinel. The presence of wüstite was detected in some of the samples when they were quickly cooled. Samples were, therefore, cooled slowly to allow wüstite to transform into magnetite during the cooling. The grain size measured for the hematite was about 270 nm, and for the magnetite, grains were horizontally 0.78  $\mu\text{m}$  and vertically 1.56  $\mu\text{m}$ .

### Exposures of Pre-oxidized Samples at 400 °C in the Absence of KCl(s): Mass Gain and Morphology

The pre-oxidized samples were investigated in a second set of exposures without KCl(s) present. The samples pre-oxidized at 500, 600, and 700 °C were exposed at 400 °C the second time. Due to spallation of the oxide scale of the reference sample and the one pre-oxidized at 700 °C, the samples were not exposed for longer times.

The samples pre-oxidized at 500 and 600 °C were exposed up to 168 h. These exposures started with oxide scales with microstructures formed at the different temperatures described above and approximately 3  $\mu\text{m}$  of thickness.

The different pre-oxidations resulted in a smaller mass gain and a slower growth rate than the non-pre-oxidized reference exposures at 400 °C; see Fig. 3a. This was expected since ions/electrons must diffuse through the pre-formed oxide scale, which continues to grow. A theoretical curve was added based on

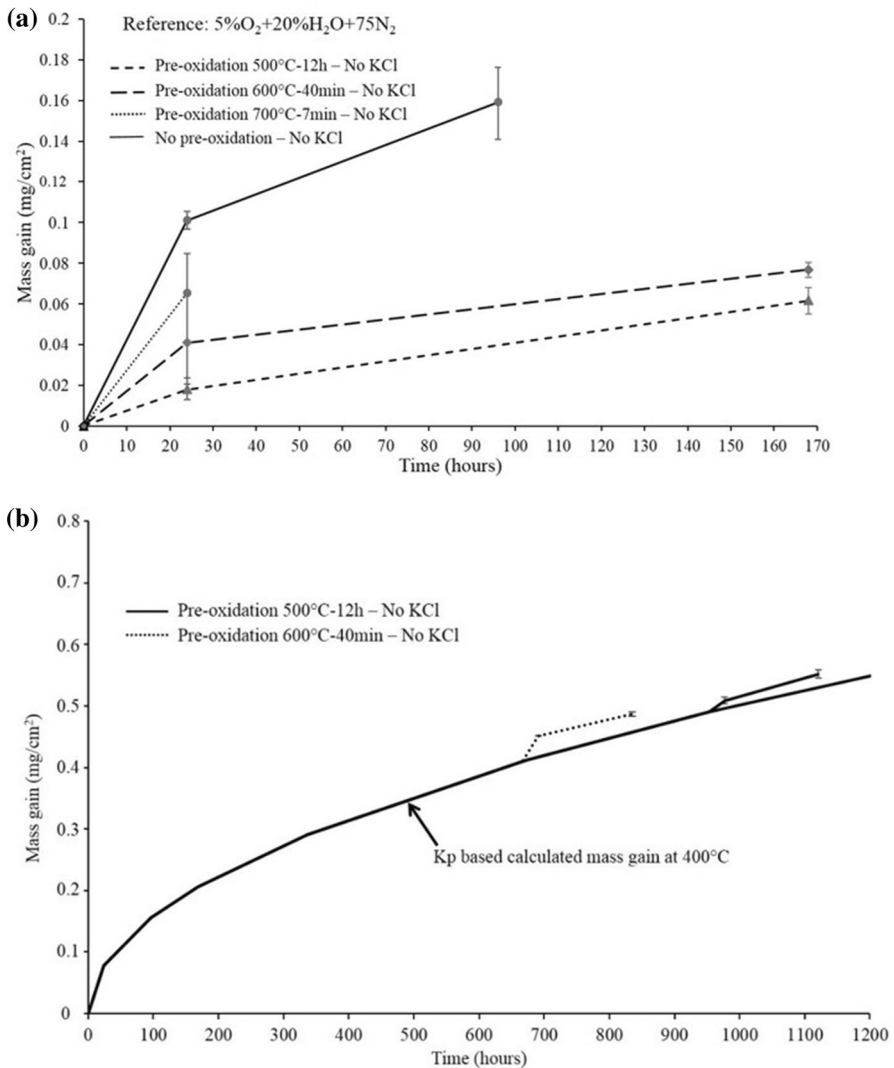


**Fig. 3** Mass gain of pre-oxidized Fe-2.25Cr-1Mo after exposure at 400 °C to 5%O<sub>2</sub> + 20%H<sub>2</sub>O + 75%N<sub>2</sub>; **a** same starting conditions considered for pre-oxidations at pre-oxidations at 500, 600, and 700 °C; **b** comparison between theoretical mass gain at 400 °C and pre-oxidations at 500 and 600 °C

the  $k_p$  value calculated for the exposure of each starting oxide scale (based on the  $k_p$  value acquired at 400 °C); see Fig. 3b. The growth rate was initially higher for the pre-oxidized samples than the expected growth rate at 400 °C; see Fig. 3b. This effect was present during the first hours of the exposure (pre-oxidation 500 °C—12 h, pre-oxidation 600 °C—40 min, and 700 °C—7 min). The deviation from the 400 °C curve was larger if the pre-oxidation temperature was higher; see Fig. 3b. Using SEM surface morphology, no indications of spallation or cracks in the pre-formed oxide scale of the reference samples were found; instead, morphology similar to the pre-formed oxide scales was observed (not shown).

### Exposures of Pre-oxidized Samples in the Presence of KCl(s) at 400 °C: Mass Gain and Morphology

In order to study the influence of KCl(s) on pre-formed iron oxide, samples pre-oxidized at 500, 600, and 700 °C were exposed at 400 °C up to 168 h in the presence of KCl(s) in a second set of exposures. The starting point of this exposure was a pre-formed oxide scale which presented an approximately 3- $\mu$ m-thick oxide scale with the microstructures described above. Non-pre-oxidized samples were exposed in the presence of KCl(s) for comparison; see Fig. 4a. The growth kinetics in the presence of KCl(s) without pre-oxidation was initially very fast. The total mass gain after 24-h exposure was 10 times higher than the reference exposure without KCl(s). All pre-oxidized samples showed less mass gain than the samples without pre-oxidation; see Fig. 4. No or very small amounts of KCl(s) were expected to evaporate at 400 °C [13].

#### Pre-oxidation Performed at 500 °C

The exposures in the presence of KCl(s) for pre-oxidation 500 °C-12 h samples resulted in a small initial increase in mass gain and eventually led to breakaway oxidation; see Fig. 4a and b. The initial mass gain was small but higher than the reference without KCl(s); see the comparison with the theoretical mass gain curve in Fig. 4b. The mass gain curve showed a significant increase in growth rate (breakaway oxidation) after an incubation time between 48 and 168 h (Fig. 4a).

Plan view images of the pre-oxidation 500 °C-12 h samples exposed for 24, 48, and 168 h in the presence of KCl(s) are shown in Fig. 5. After 24 h, the pre-oxidation 500 °C-12 h sample showed a surface morphology consisting of base oxide and oxide around KCl(s) particles. The mass gain after 24 h was low, which is in good agreement with surface morphology shown in Fig. 5a. The surface morphology consisted of iron oxide between the still principally unreacted KCl(s) particles after a 48-h exposure; see Fig. 5b. After 168 h, however, a widespread attack occurred. All observed KCl(s) particles were consumed, and the surface morphology had become an undulating iron-rich oxide over surface; see Fig. 5c. Quantitative SEM/EDX analysis indicated the presence of small amounts of KCl(s) on some areas of the surface. The whisker-type morphology reported after pre-oxidation was not observed,

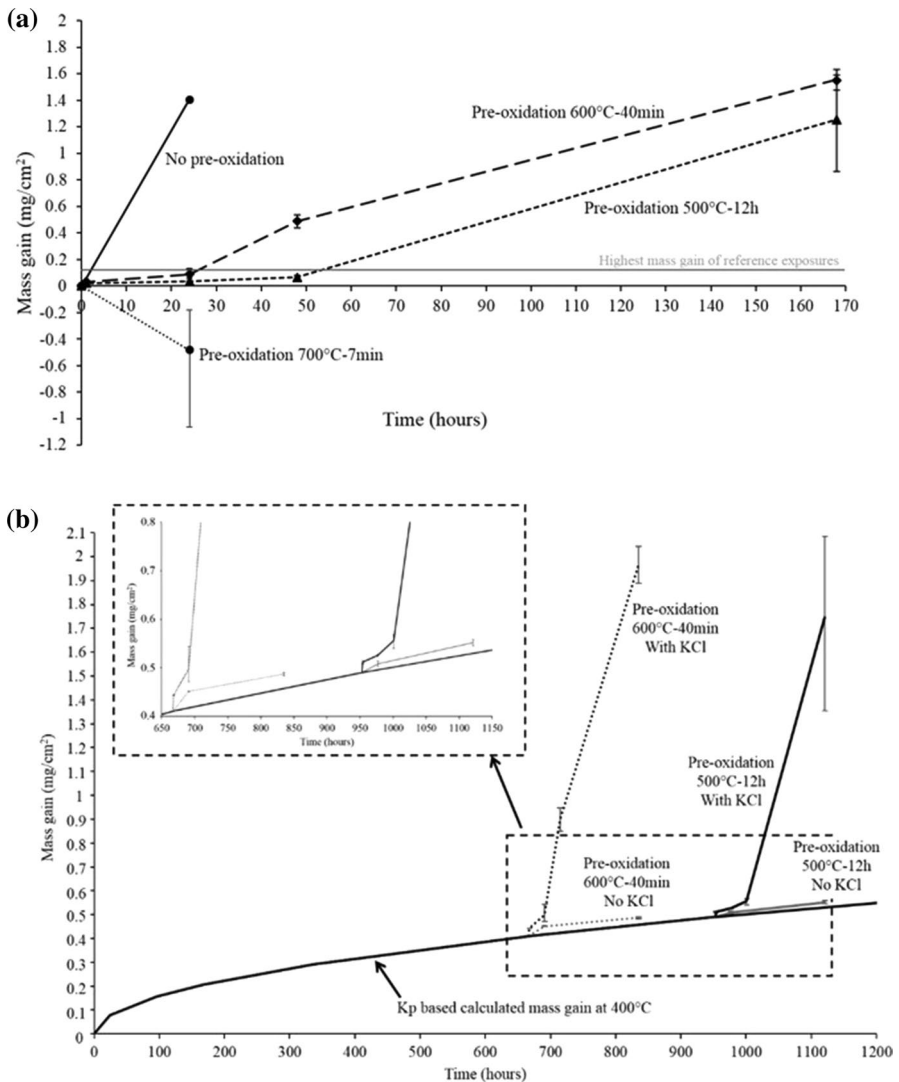


**Fig. 4** Mass gain of pre-oxidized Fe-2.25Cr-1Mo after exposure at 400 °C to 5%O<sub>2</sub> + 20%H<sub>2</sub>O + 75%N<sub>2</sub> in presence of 0,1 mg/cm<sup>2</sup> KCl(s); **a** same starting conditions considered for pre-oxidations at pre-oxidations at 500, 600, and 700 °C; **b** comparison between theoretical mass gain at 400 °C and pre-oxidations at 500 and 600 °C

but areas with thick iron oxide on the former KCl(s) particles were observed; see Fig. 5c. This morphology is in good agreement with the mass gain data (Fig. 4a), which indicates breakaway oxidation.

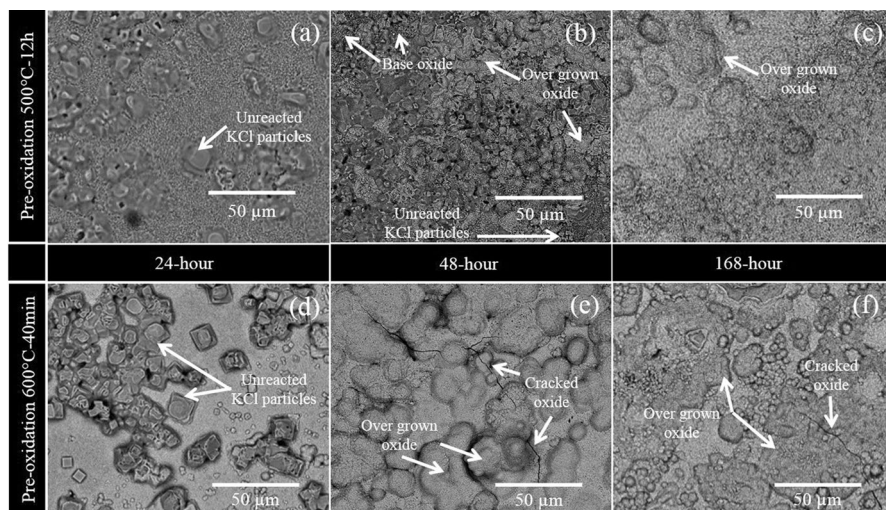


**Fig. 5** BSE images of plan view of pre-oxidized Fe-2.25Cr-1Mo after exposure at 400 °C to 5%O<sub>2</sub> + 20%H<sub>2</sub>O + 75%N<sub>2</sub> + 0.1 mg/cm<sup>2</sup> KCl(s); pre-oxidation 500 °C-12 h: **a** 24 h, **b** 48 h, **c** 168 h; pre-oxidation 600 °C-40 min: **d** 24 h, **e** 48 h, **f** 168 h

### Pre-oxidation Performed at 600 °C

The samples exposed in the presence of KCl(s) for pre-oxidation 600 °C-40 min resulted in a small initial increase in mass gain and eventually led to breakaway oxidation; see Fig. 4a and b. The mass gain curve shows that the initial mass gain is higher than for the reference case without KCl(s) prior to breakaway oxidation, compare Figs. 3a and 4a. After 24 h, the mass gain was low which is in good agreement with surface morphology; see Fig. 5. The surface morphology of the sample after a 24-h exposure was similar to the base oxide formed prior to KCl(s) exposure. Unreacted KCl(s) particles were also observed; see Fig. 5d.

After a 24-h exposure, the mass gain showed a dramatic increase in corrosion rate; see Fig. 4a and b. The sample surface was in good agreement with the mass gain and consisted of former KCl(s) particles overgrown with iron oxide. No or very small amounts of unreacted KCl(s) particles were observed. After a 168-h exposure, the undulating sample surface contained some cracks and some spalled regions; see Fig. 5f. Former KCl(s) particles were overgrown with iron oxide-containing traces of KCl(s); see Fig. 5d–f.

### Pre-oxidation Performed at 700 °C

The samples exposed in the presence of KCl(s) for pre-oxidation 700 °C-7 min resulted in breakaway oxidation during the initial 24 h of the exposure; see Fig. 4a. This resulted in oxide spallation as early as after 24 h, which gives mass loss; see Figs. 4a and 6a. The morphology investigation indicated that the spallation occurred

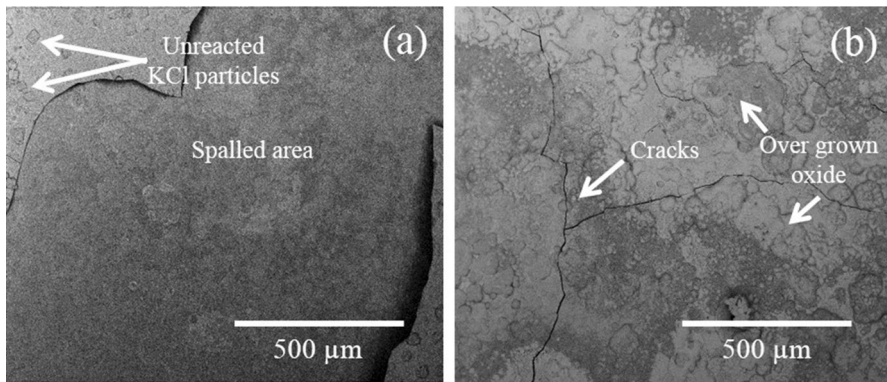


**Fig. 6** BSE images of plan view of pre-oxidation 700 °C-7 min Fe-2.25Cr-1Mo after 24 h exposure at 400 °C to 5%O<sub>2</sub> + 20%H<sub>2</sub>O + 75%N<sub>2</sub> + 0.1 mg/cm<sup>2</sup> KCl(s); **a** oxide spallation area, **b** oxide cracked area

both during the exposure (partly overgrown regions) and during cooling. Due to the initial fast spallation of the oxide scale, longer time exposures were not performed.

### Exposures of Pre-oxidized Samples in the Presence of KCl(s) at 400 °C: Oxide-Scale Microstructure

The investigation of mass gain and surface morphology showed continued oxide growth with almost no differences for the reference case. However, the impact of KCl(s) was larger and strongly dependent on pre-oxidation temperature; see Fig. 4a and b. The microstructural investigation was, therefore, focused on the samples exposed in the presence of KCl(s).

#### Pre-oxidation Performed at 500 °C

The oxide microstructure of the samples exposed to pre-oxidation 500 °C-12 h in the presence of KCl(s) at 400 °C was investigated after 24 and 48 h (before break-away oxidation) and after 168 h (after breakaway). Figure 7a–c shows ion-milled cross-sectional SEM images of pre-oxidations samples 500 °C-12 h after exposure in presence of KCl(s). After 24 h, the pre-formed oxides were still adherent and homogenous; see Fig. 7a. A small increase in oxide scale thickness compared to the initial pre-formed oxide scales was observed after exposure to KCl(s), which is in good agreement with mass gain; see Fig. 4a. The total oxide-scale thickness increased about 0.9 μm, and the proportion of the oxides in the scale corresponded to 20% hematite, 50% magnetite, and 30% iron chromium spinel.

After a 48-h exposure, the oxide scale remained uniform and well attached to the metal. The morphology and microstructure of the oxide scale were similar to those observed after 24 h; see Fig. 7a and b. However, the investigation into microstructure indicated that the oxide layer was denser than the sample exposed for 24 h, i.e., contained fewer pores. The thickness of the oxide scale showed a small/almost no increase. The proportion of the oxides present in the scale changed to approximately



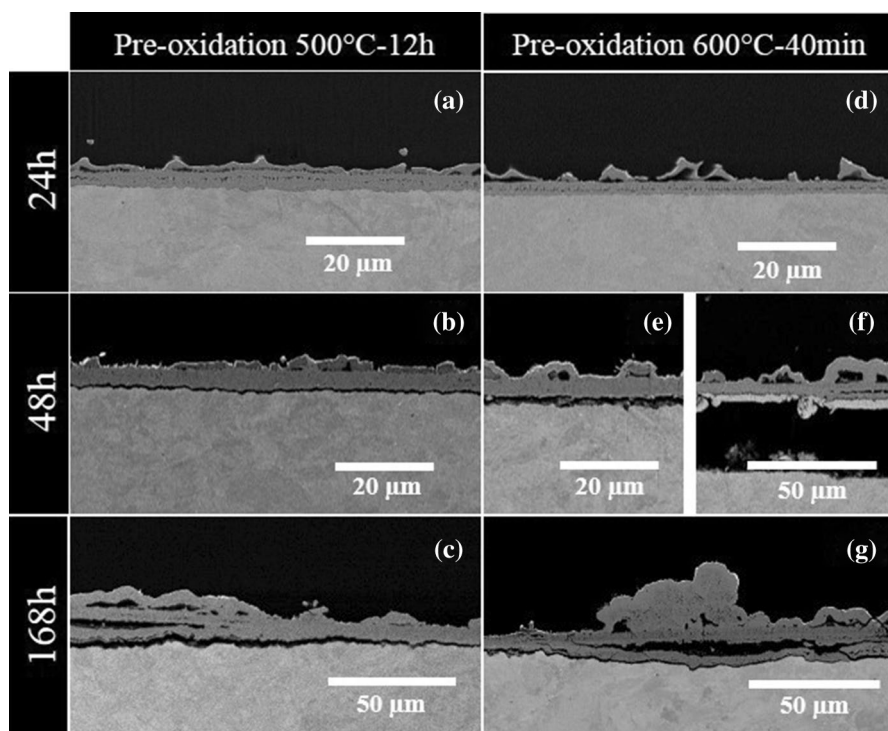


**Fig. 7** BSE images of cross sections of pre-oxidized Fe–2.25Cr–1Mo after 24-, 48-, and 168-h exposure at 400 °C to 5%O<sub>2</sub> + 20%H<sub>2</sub>O + 75%N<sub>2</sub> + 0.1 mg/cm<sup>2</sup> KCl(s); pre-oxidation 500 °C–12 h: **a** 24 h, **b** 48 h, **c** 168 h; pre-oxidation 600 °C–40 min: **d** 24 h, **e** 48 h, **f** 168 h

13% hematite, 58% magnetite, and 29% iron chromium spinel. After 168 h, the samples had suffered from breakaway corrosion, i.e., the oxide scale had become thicker than the sample exposed for 48 h (Fig. 7c), which is in good agreement with mass gains; see Fig. 4a. The oxide scale was partially detached and cracked. The outward-growing oxide was observed to be denser than the initial pre-oxidations in the regions where the oxide was attached; see Figs. 2a and 8a. The total thickness of the oxide scale was found to increase, on average, to 6–7 μm; the measurement varied due to the formation of blisters in different regions of the oxide scale; see Fig. 7c. The presence of metal chlorides at the metal–oxide interface in regions where the oxide scale remained attached is shown in Fig. 8a, and this was confirmed by using EDX analysis (not shown).

### Pre-oxidation Performed at 600 °C

The microstructure of the pre-oxidation 600 °C–40 min exposures in the presence of KCl(s) was investigated after 24 h (before breakaway oxidation) and after 48 h (after breakaway). Figure 7d–g shows ion-milled cross-sectional SEM images of pre-oxidations 600 °C–40 min after exposure in presence of KCl(s). After 24 h, the pre-formed

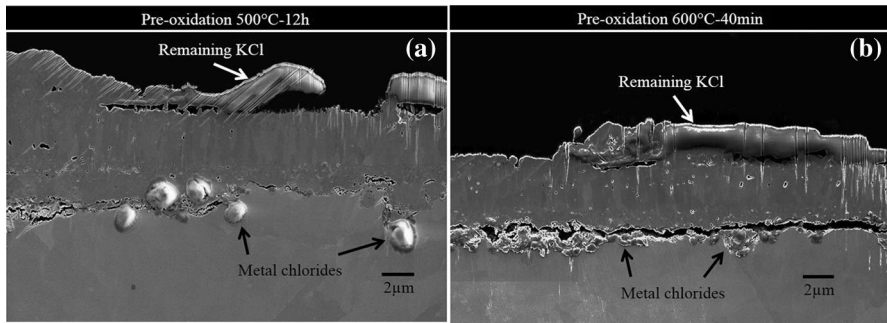


**Fig. 8** SE image of cross sections of pre-oxidized Fe-2.25Cr-1Mo after 168-h exposure at 400 °C to 5%O<sub>2</sub> + 20%H<sub>2</sub>O + 75%N<sub>2</sub> + 0.1 mg/cm<sup>2</sup> KCl(s); **a** pre-oxidation 500 °C-12 h, **b** pre-oxidation 600 °C-40 min

oxide 600 °C-40 min was still adherent with a homogenous thickness; see Fig. 7d. A very small increase in oxide scale thickness was observed which agrees with the mass gain reported. The total thickness increased about 0.3 μm; the proportion of the oxides in the scale corresponds to 15% hematite, 62% magnetite and 23% iron chromium spinel.

After a 48-h exposure, the oxide scale had become detached in some regions, and the presence of chlorine was detected at the metal–oxide interface; see Fig. 7e and f. In regions where the oxide scale remained attached, the oxide scale was denser, and the thickness of the scale was greater than after a 24-h exposure. According to measurements of still attached oxide scale, the thickness increased by about 0.9 μm compared to the pre-formed scale before exposure. The proportion of the oxides in the scale was approximately 13% hematite, 63% magnetite, and 24% iron chromium spinel. After 168 h, the oxide scale had become partially detached and cracked; see Figs. 5f and 7g; however, in some regions, the oxide was attached and dense; see Fig. 8. The total thickness of the oxide scale was, on average, 10 μm. According to the EDX analysis (not shown), metal chlorides were detected at the metal–oxide interface on both pre-oxidized samples; see Fig. 8. Due to the breakaway of the oxide scale, the measurements varied from region to region on the samples exposed for 48 and 168 h.

### Impact of KCl(s) on Pre-oxidation Performed at 700 °C

The microstructure of the sample for pre-oxidation 700 °C-7 min exposed in the presence of KCl(s) was not investigated in detail due to spallation of the oxide scale; see Fig. 6.

## Discussion

The aim of this work was to investigate the influence of oxide-scale microstructure on the corrosion of low-alloyed steels in the absence and presence of KCl(s). This was achieved with well-controlled pre-oxidation procedures performed at different



temperatures and times and exposed with and without KCl(s) at 400 °C. Detailed microstructural investigations were used to examine the influence of temperature on the different pre-oxidation scales.

### Pre-oxidation Parameters: Influence of Temperature on Oxidization Kinetics and Microstructure

The oxide kinetics and oxide microstructure of the Fe–2.25Cr–1Mo alloy was investigated at different temperatures during the pre-oxidation stage. The parabolic rate constant ( $k_p$ ) values varied from  $6 \times 10^{-12}$  at 500 °C,  $8 \times 10^{-11}$  at 600, and  $5 \times 10^{-6}$  at 700 °C. This is in good agreement with reports in the literature [17]. The growth kinetics were in the same range as for the oxide scales formed on pure iron at 400 and 500 °C [17, 21]; any difference might be due to the different contents of water vapor in the oxidation atmosphere and chromium content in the alloy. All characterized oxide scales consisted of an outward-growing hematite ( $\text{Fe}_2\text{O}_3$ ) layer on top, a middle layer of magnetite ( $\text{Fe}_3\text{O}_4$ ), and an inward-growing iron chromium spinel ( $(\text{Fe,Cr})_3\text{O}_4$ ); see Fig. 2. Wüstite is expected to form at a temperature above 573 °C during the oxidation of pure iron; however, the presence of chromium in the alloy shifted the formation of Wüstite toward higher temperatures [22]. This is in good agreement with the oxide-scale microstructure reported to form on iron, FeCr model and commercial alloys, and low-alloyed steels [13, 14, 16, 17, 23, 24] and the scale formed at 600 °C; see Fig. 2. The samples pre-oxidized at 700 °C may form wüstite and therefore show a larger difference between calculated and measured thicknesses. This difference of calculated and measured thickness could have been caused by the presence of wüstite (calculations made assuming magnetite), uneven growth or spalled regions. The characterized samples did not show presence of wüstite (with a low cooling rate); see Fig. 2c, and plan view investigations did not reveal any signs of spallation or very undulating surface even though this could be difficult to observe.

Exposure times were, based on the oxide kinetics at different temperatures, selected to produce scale thicknesses in the same range but formed at different temperatures and exposure times; see Figs. 1 and 2. The surface morphology of the hematite changed with pre-oxidation temperature. Whiskers formed on the hematite surface of the pre-oxidation 500 °C–12 h in the presence of water vapor, which was not observed on the pre-oxidations 600 °C–40 min and 700 °C–7 min samples. A similar phenomenon was observed by Pujilaksono, et al. [17] when oxidizing pure iron in the presence of 40% water vapor. Those authors have suggested that, at 400 and 500 °C, the weakening of the  $\text{Fe}^{3+}$  ions on the hematite surface and the oxygen ions below the surface is caused by the presence of water vapor, which promotes the mobilization of iron ions on the surface and results in the formation of whiskers [17]. The effect of water vapor has been found to have an impact on iron oxide growth rate at 500 and 600 °C, while no effect has been observed at 400 °C [17]. It is also important to notice the different times required to achieve similar oxide-scale thicknesses as there could be an incubation time prior to growth of whiskers. A difference in morphology may influence the distribution of KCl(s) during

the preparation of the second exposure step even though this was not seen in the plan view images; see Fig. 5. Besides the difference in morphology, there was a minor difference in the thicknesses of the pre-oxidations performed at different temperatures according to calculated thicknesses: 500 °C–12 h (3.4  $\mu\text{m}$  and 2.6–4.0  $\mu\text{m}$  spread), 600 °C–40 min (3.0  $\mu\text{m}$  and 2.4–3.3  $\mu\text{m}$  spread), and 700 °C–7 min (3.7  $\mu\text{m}$  and 3.3–4.1  $\mu\text{m}$  spread). The hematite layer had a similar thickness on all samples at all temperatures, however, with a different oxide grain size, i.e., the smallest oxide grains at 500 °C (150 nm) and largest at 700 °C (270 nm). The variation in thickness between the different environments is summarized in Table 2.

### **Influence of Pre-oxidization on Oxidation in 5%O<sub>2</sub> + 20%H<sub>2</sub>O + 75%N<sub>2</sub> at 400 °C**

The pre-oxidations resulted in different oxide-scale microstructures and a small difference in thickness, as described above. When the pre-oxidized samples were exposed without KCl(s) at 400 °C, a lower oxidation rate was observed compared to the non-pre-oxidized samples in all cases; see Fig. 3a. The difference in the pre-oxidation thickness of the oxide scales influences the growth rate of the same. In order to neutralize the difference in starting thickness, the mass gains were compared to a calculated mass gain curve based on the exposures performed at 400 °C; see Fig. 3b. Samples pre-oxidized at higher temperatures showed higher corrosion rates than the theoretical mass gain curve; see Fig. 3b. Thus, the results indicate that oxide-scale microstructure, phase distribution, and thickness have an influence on the growth rate of the pre-formed oxides when oxidized at 400 °C. Factors besides thickness that may influence the properties of the scale are the distribution of the different phases (Fe<sub>2</sub>O<sub>3</sub>, Fe<sub>3</sub>O<sub>4</sub>, and FeO), the density of grain boundaries, pore formation, and/or the defect chemistry of the oxides. The examination of microstructure showed that the hematite layer had a similar thickness in all pre-oxidations, while the magnetite layer differed more; see Fig. 2. However, there is no clear correlation between grain size and growth rate in this case as the sample with the largest oxide grains had the fastest growth rate. It should also be noted that the initial growth rate at 400 °C was higher than expected for all cases; see Fig. 3b, while no signs of cracks or spallation were found on the samples.

### **Influence of KCl(s) at 400 °C on the Oxidation of Low-Alloyed Steels (No Pre-oxidation)**

It is well known that alkali chlorides accelerate the corrosion of low-alloyed steels in the temperature range 300–500 °C [2–5, 9–15, 25]. Alkali salts, e.g., KCl(s) and NaCl(s), have been shown to accelerate the oxidation rate of the low-alloyed steel Fe–2.25Cr–1Mo, forming a non-protective porous oxide scale at 400 and 500 °C. The growth rate has been reported to follow a growth rate much faster than the corresponding exposure without KCl(s) [13, 15, 25]. After 24 h, the sample without pre-oxidation showed a mass gain similar to the mass gain obtained for pre-oxidized samples after a 168-h exposure; see Fig. 4a. The uniform corrosion attack is suggested to be caused by the rapid reaction of KCl(s) with the metal (starting at

355 °C) [14]. This is in good agreement with the reference samples exposed without pre-oxidation.

### **Influence of Pre-oxidization on Oxidation in 5%O<sub>2</sub> + 20%H<sub>2</sub>O + 75%N<sub>2</sub> with KCl(s) at 400 °C**

Chlorine is expected to penetrate the pre-formed oxide scales in the presence of KCl(s), either as a gas or as diffusing species [3, 13, 15, 18]. Whether chlorine penetrates as a gas or as diffusing species, it is expected to have an incubation time on a pre-formed oxide scale, while this is not expected for a non-pre-oxidized sample. The mass gain data (Fig. 4a, b) show, as expected, an incubation time followed by breakaway oxidation in the presence of KCl(s), while the exposures of the non-pre-oxidized low-alloyed steels had a swift onset of rapid corrosion in the presence of KCl(s); see Fig. 4a. Pre-oxidation samples 500 °C-12 h and 600 °C-40 min also showed unreacted KCl(s) particles after the first hours of exposure, while all KCl(s) particles had been consumed after breakaway oxidation; see Fig. 5. The surface morphology of the exposed samples can be explained by slow surface transport due to the absence or very low levels of FeCl<sub>2</sub> and, thereby, the eutecticum on the already pre-formed oxide scales, which leads to a more local corrosion attack; see Fig. 8. Both pre-oxidation samples 500 °C-12 h and 600 °C-40 min behaved similarly during the first hours of exposure in the presence of KCl(s), i.e., they showed slow growth kinetics; see Fig. 4a. The mass gains of the samples exposed in the presence of KCl(s) were higher than for the reference samples prior to breakaway; see Fig. 4a and b. A change in microstructure preceding breakaway oxidation was also found in the investigation. The scales appeared to be denser with fewer pores prior to breakaway oxidation; see Fig. 8. The mechanism of pore formation in iron oxide has been studied by Ueda et al. [26], who simulated pore formation and distribution with chemical potential distribution, the flux of the oxide ion and its divergence. Thus, the results indicate a change in ion diffusion in the presence of KCl(s) preceding breakaway oxidation.

An increase in corrosion rate, i.e., breakaway corrosion, was observed as early as after 24 h of exposure for the 600 °C-40 min sample. This can be compared to the pre-oxidation 500 °C-12 h sample in which an increase in corrosion rate occurred after 48 h. The 700 °C-7 min sample, with the thickest pre-formed oxide scale, showed the fastest corrosion rate in the reference exposure; see Figs. 3a and 4a. This sample also had the shortest incubation time to breakaway in the presence of KCl(s), i.e., less than 24 h. The grain size of the hematite and magnetite was measured; see Table 2. It was expected that smaller grains would result in diffusion of more Cl<sup>-</sup> ions and thereby shorter incubation time to breakaway oxidation. However, in this study, this correlation between grain sizes and incubation time to breakaway oxidation was not observed.

The microstructure of the 500 °C-12 h and 600 °C-40 min samples after breakaway oxidation was characterized, and the presence of metal chlorides in the metal/oxide interface was observed; see Fig. 8. Cracks could be seen in some positions, but the investigation indicated that they formed after the exposures; see Fig. 7.

The influence of pre-oxidation in the presence of alkali chlorides has been studied earlier by Reese et al. [15]. In their work, the thickness of the pre-formed oxide scales was very thick, i.e., between 40 and 190  $\mu\text{m}$ . The samples exposed in the presence of alkali chloride ( $\text{NaCl(s)}$ ) showed that a thicker pre-formed oxide experienced a lower corrosion rate. This is in agreement with the results of the present study, even though the oxide scales were much thinner. Parallel to the current study, the effect of oxide-scale thickness on the corrosion attack induced by  $\text{KCl(s)}$  has been investigated Andersson and Alhede [27]. The authors produced oxide scales with thickness between 2 and 13  $\mu\text{m}$  (calculated) and exposed in the presence of  $\text{KCl(s)}$  in the same conditions as the present study. According to Andersson, it was confirmed that differences in the thickness of the pre-formed oxide scale has an influence on the further corrosion attack, i.e., incubation time to breakaway.

## Conclusions

Metallic parts of boilers suffer from aggressive corrosion attacks in the complex environment generated during the combustion of biomass and waste. The alloys used for those components usually form an oxide scale during the first operation hours of the boiler. These oxide scale and alloy material are the starting condition for the propagation of a more aggressive corrosion attack. The aim of this study was to investigate the influence of the oxide-scale microstructure formed during the first hours of operation.

The findings indicate that resistance toward chlorine-induced corrosion is a combination of oxide-scale thickness and microstructure. However, there is no direct correlation between the thickness of hematite layer and its grain size with the incubation time to breakaway oxidation. However, the microstructural investigation found that the breakaway mechanism is diffusion-controlled as pore formation changes prior to breakaway oxidation. High-resolution microscopy in combination with TG would be needed to further investigate the influence of oxide microstructure and the changes on chlorine-induced corrosion.

**Acknowledgements** This work was carried out at the Swedish High Temperature Corrosion Centre (HTC) at Chalmers University of Technology. The authors would like to thank Jakob Dahlqvist for preparing samples and performing part of the exposures.

**Open Access** This article is distributed under the terms of the Creative Commons Attribution 4.0 International License (<http://creativecommons.org/licenses/by/4.0/>), which permits unrestricted use, distribution, and reproduction in any medium, provided you give appropriate credit to the original author(s) and the source, provide a link to the Creative Commons license, and indicate if changes were made.

## References

1. H. P. Nielsen, F. J. Frandsen, K. Dam-Johansen and L. L. Baxter, *Progress in Energy and Combustion Science*. **26**, 283 (2000).
2. S. C. Cha and M. Spiegel, *Materials and Corrosion*. **57**, 159 (2006).
3. H. J. Grabke, E. Reese and M. Spiegel, *Corrosion Science* **37**, 1023 (1995).

4. Y. S. Li, Y. Niu and W. T. Wu, *Materials Science and Engineering a-Structural Materials Properties Microstructure and Processing* **345**, 64 (2003).
5. H. T. Ma, C. H. Zhou and L. Wang, *Corrosion Science* **51**, 1861 (2009).
6. S. Sroda, M. Makipaa, S. Cha and M. Spiegel, *Materials and Corrosion* **57**, 176 (2006).
7. S. Sroda and S. Tuurna, *Materials and Corrosion* **57**, 244 (2006).
8. S. Sroda, S. Tuurna, K. Penttila and L. Heikinheimo, *Materials Science Forum*. **461–464**, 981 (2004).
9. M. A. Uusitalo, P. M. J. Vuoristo and T. A. Mantyla, *Materials Science and Engineering a-Structural Materials Properties Microstructure and Processing*. **346**, 168 (2003).
10. M. A. Uusitalo, P. M. J. Vuoristo and T. A. Mantyla, *Corrosion Science* **46**, 1311 (2004).
11. F. Wang and Y. Shu, *Oxidation of Metals* **59**, 201 (2003).
12. A. Zahs, M. Spiegel and H. J. Grabke, *Corrosion Science* **42**, 1093 (2000).
13. N. Folkesson, T. Jonsson, M. Halvarsson, L. G. Johansson and J. E. Svensson, *Materials and Corrosion-Werkstoffe Und Korrosion*. **62**, 606 (2011).
14. T. Jonsson, N. Folkesson, J. E. Svensson, L. G. Johansson and M. Halvarsson, *Corrosion Science* **53**, 2233 (2011).
15. E. Reese and H. J. Grabke, *Materials and Corrosion* **43**, 547 (1992).
16. B. Pujilaksono, T. Jonsson, H. Heidari, M. Halvarsson, J. E. Svensson and L. G. Johansson, *Oxidation of Metals* **75**, 183 (2011).
17. B. Pujilaksono, T. Jonsson, M. Halvarsson, J.-E. Svensson and L.-G. Johansson, *Corrosion Science* **52**, 1560 (2010).
18. N. Folkesson, L.-G. Johansson and J.-E. Svensson, *Journal of The Electrochemical Society* **154**, C515 (2007).
19. B. Lalgudi Srinivas. Experimental evaluation of oxide growth in binary zirconium alloys along with pure zirconium and Zircaloy-2 by steam corrosion testing (2012).
20. B. W. S. Kempshall and S. M. Schwarz, *Journal of Vacuum Science & Technology B: Microelectronics and Nanometer Structures Processing, Measurement, and Phenomena*. **19**, 749 (2001).
21. T. Jonsson, B. Pujilaksono, A. Fuchs, J. E. Svensson, L. G. Johansson and M. Halvarsson, *The influence of H<sub>2</sub>O on iron oxidation at 600 C: a microstructural study*, (Trans Tech Publ, Materials Science Forum, City, 2008), p. 1005.
22. A. S. Khanna. *Introduction to High Temperature Oxidation and Corrosion*, (City: ASM International, 2002).
23. T. Jonsson, B. Pujilaksono, S. Hallström, et al., *Corrosion Science* **51**, 1914 (2009).
24. T. Jonsson, B. Pujilaksono, H. Heidari, et al., *Corrosion Science* **75**, 326 (2013).
25. E. Reese and H. J. Grabke, *Materials and Corrosion* **44**, 41 (1993).
26. M. Ueda, K. Kawamura, T. Maruyama. Void formation in magnetite scale formed on iron at 823 K-Elucidation by chemical potential distribution. *Materials science forum*, City; Trans Tech Publ;37–44 (2006).
27. R. Andersson and A. Alhede, *The effect of oxide scale thickness on the KCl-induced corrosion of a low-alloyed steels at 400°C*, (Chalmers University of Technology, City, 2017).